



Laser-structured Janus wire mesh for efficient oil–water separation†

Cite this: *Nanoscale*, 2017, **9**, 17933

Yu-Qing Liu,^a Dong-Dong Han,^a Zhi-Zhen Jiao,^a Yan Liu,^b Hao-Bo Jiang,^b Xuan-Hang Wu,^a Hong Ding,^c Yong-Lai Zhang  *^a and Hong-Bo Sun  ^{a,d}

We report here the fabrication of a Janus wire mesh by a combined process of laser structuring and fluorosilane/graphene oxide (GO) modification of the two sides of the mesh, respectively, toward its applications in efficient oil/water separation. Femtosecond laser processing has been employed to make different laser-induced periodic surface structures (LIPSS) on each side of the mesh. Surface modification with fluorosilane on one side and GO on the other side endows the two sides of the Janus mesh with distinct wettability. Thus, one side is superhydrophobic and superoleophilic in air, and the other side is superhydrophilic in air and superoleophobic under water. As a proof of concept, we demonstrated the separation of light/heavy oil and water mixtures using this Janus mesh. To realize an efficient separation, the intrusion pressure that is dominated by the wire mesh framework and the wettability should be taken into account. Our strategy may open up a new way to design and fabricate Janus structures with distinct wettability; and the resultant Janus mesh may find broad applications in the separation of oil contaminants from water.

Received 17th August 2017,
Accepted 18th October 2017

DOI: 10.1039/c7nr06110b

rscl.li/nanoscale

Introduction

Efficient oil–water separation has long been considered an important issue, since the frequently occurring oil spillage events and the industrial wastewater discharge continuously threaten the aqueous environment, even affecting human health.^{1–5} Currently, there exist several strategies that enable controllable oil–water separation.^{6,7} For instance, porous materials with high surface areas and large pore volumes have been used for oil adsorption.^{8,9} To avoid being saturated with water, some superhydrophobic nanoporous polymers and sponges have been successfully prepared for oil–water separation.^{10,11} Despite the fact that the selective adsorption of oil has been achieved, the limited adsorption volume and the complex regeneration procedures significantly restrict their practical applications.

Considering the distinct difference in surface tension between water (72.8 mN m⁻¹) and oil (<30 mN m⁻¹), mesh

membranes with unique dewetting properties have emerged as an appealing alternative for rapid oil–water separation.^{12,13} Typically, based on the comparison between oil density and water density ($\rho_{\text{oil}} > \rho_{\text{water}}$ or $\rho_{\text{oil}} < \rho_{\text{water}}$), the mesh membranes for oil–water separation can be simply classified into two categories: the superhydrophobic/oleophilic mesh membranes and the hydrophilic but under-water superoleophobic mesh membranes. The former realize oil–water separation by unidirectional oil transportation since water cannot pass through the mesh due to its superhydrophobicity; whereas the latter separate oil from water by discharging water, because oils that are lighter than water cannot permeate through the superoleophobic water/mesh interface. To date, wire meshes have been decorated with various nanomaterials with rough nanostructures to realize such superhydrophobicity or under-water superoleophobicity.^{14–16} For example, Jiang *et al.* first reported the fabrication of poly(tetrafluoroethylene)-coated mesh by a very simple spray-and-dry method.¹⁷ The resultant mesh is both superhydrophobic and superoleophilic, and thus enables oil–water separation. After that, various functional materials, such as polymers, boron nitride nanotubes, metals, metal oxides and carbon, have been coated on mesh membranes and applied for oil–water separation.^{18,19} The basic principle is creating a superhydrophobic and superoleophilic surface on the wire mesh. In this way, unidirectional oil transportation can be realized. Inspired by fish scales that exhibit a unique anti-oil property in water due to the presence of water-phase micro/nano hierarchical structures on the surface, functional

^aState Key Laboratory on Integrated Optoelectronics, College of Electronic Science and Engineering, Jilin University, 2699 Qianjin Street, Changchun 130012, China. E-mail: yonglaizhang@jlu.edu.cn

^bKey Laboratory of Bionic Engineering (Ministry of Education), Jilin University, Changchun, 130022, China

^cState Key Laboratory of Inorganic Synthesis and Preparative Chemistry, College of Chemistry, Jilin University, Changchun, 130012, China

^dDepartment of Precision Instrument, Tsinghua University, Beijing, 100084, China

†Electronic supplementary information (ESI) available. See DOI: 10.1039/c7nr06110b

mesh membranes with superhydrophilicity in air and superoleophobicity in water have also been developed for oil–water separation.^{20,21} Compared with the superhydrophobic mesh, the under-water superoleophobic mesh is more workable in practical oil–water separation. Since most oils are lighter than water, the mesh will probably come into contact with water first in the case of gravity-induced oil–water separation. Clearly, discharging the water is a preferred method. According to a simple principle that the superhydrophilic solid surface in air is crucial to the under-water superoleophobicity at the water/solid interface, hydrophilic materials including hydrogels, metal oxides, zeolites and graphene oxides have been coated on wire meshes for developing oil–water separation membranes.^{22,23}

As mentioned above, rapid progress has been made in this dynamic field so far. However, both of these kinds of oil–water separation mesh/membranes are not universally applicable. Each kind of mesh is only suitable for a certain case, and it further depends on the density of the oils ($\rho_{\text{oil}} > \rho_{\text{water}}$ or $\rho_{\text{oil}} < \rho_{\text{water}}$). More importantly, both of them are incapable of unidirectional transport of oils or water. Inverse flow would not only lower the separation efficiency, but also result in a poor separation selectivity in the real separation process. Recently, Janus membranes with asymmetric dewetting properties on both sides have emerged as a solution to the above-mentioned problems.^{24,25} However, in most cases, the Janus membranes were prepared by the selective modification of one side, sequential decoration, or directly combining two membranes together. To achieve distinct wetting behaviours on the two sides of the Janus wire mesh, it is necessary to get precise control over the surface micronanostructures and the chemical composition on both sides synchronously, while currently, it is still challenging to attain this.

We report in this paper a laser structuring method to make a Janus wire mesh for efficient oil/water separation. Janus structures have been realized through laser treatments under different laser intensities and selective modification of the two sides using fluorosilane and graphene oxide (GO), respectively. The resultant Janus mesh shows asymmetric wetting properties, a superhydrophobic/superoleophilic side and a superhydrophilic but underwater superoleophobic side. Using this Janus mesh, the separation of different oils (both light oil and heavy oil) from water has been demonstrated, in which high separation efficiencies have been achieved. The present work may open up a new way to design and fabricate Janus structures towards wettability-oriented applications.

Experimental

Preparation of superhydrophobic side of the wire mesh

A Cu wire mesh with an average pore size of $150 \times 150 \mu\text{m}$ and a wire diameter of $100 \mu\text{m}$ was used for laser structuring (@580 mW, $7.39 \times 10^6 \text{ mJ cm}^{-2}$). 1H,1H,2H,2H-Perfluorodecyltriethoxysilane (96%, Aladdin) was used to

prepare superhydrophobic wire meshes in a sealed reaction kettle at $95 \text{ }^\circ\text{C}$ for 12 h.

Preparation of under-water superoleophobic side of the wire mesh

We made LIPSS structures on the back side using a laser fluence of $12.74 \times 10^5 \text{ mJ cm}^{-2}$ (100 mW), at a scanning speed of 2 mm s^{-1} . GO was prepared using a modified Hummers method. The back side of the wire mesh was dip coated in a GO aqueous solution and dried in air for further use.

Characterization

The wettability of the Janus mesh was measured by using a Contact Angle System OCA 20 (DataPhysics Instruments GmbH, Germany) at ambient temperature. The CAs of various oils and organic reagents were measured with a droplet of $4 \mu\text{L}$. SEM images were obtained by using a field emission scanning electron microscope (JSM-7500F, JEOL, Japan). Confocal laser scanning microscope (CLSM) images were captured using a LEXT 3D measuring laser microscope (OLS4100). XPS was performed using an ESCALAB 250 spectrometer. FTIR spectra were recorded on an IFS 66 V S^{-1} (Bruker) IR spectrometer in the range $400\text{--}2000 \text{ cm}^{-1}$.

Results and discussion

Fabrication of Janus wire meshes

We fabricated the Janus meshes by sequential laser structuring and surface modification using fluorosilane and GO, respectively. Fig. 1 shows the schematic illustration of the fabrication procedures. To make rough micronanostructures on the Cu wire mesh, femtosecond laser processing was employed. Laser-induced periodic surface structures (LIPSS) formed due to the optical interference between the incident laser radiation and a surface electromagnetic wave (SEW). The formation of LIPSS makes the surfaces of the wires very rough. To further promote the surface dewetting properties, we modified it with fluorosilane. In this way, the wire mesh became superhydrophobic (water contact angle, CA = 160°). Here, it is worth pointing out that we do not have to control the modification on only one side, since the back side has to sustain another laser treatment. In this way, the residual fluorosilane on the back side would be totally removed. Interestingly, by simply controlling the laser intensity, a worm-like ripple structure would form on the back side providing a relatively weak laser intensity is used. To endow the surface with a distinct dewetting property, we modified it with a hydrophilic GO. It is well known that the superhydrophilicity of a surface at the air/solid interface is crucial to the superoleophobicity at the water/solid interface. GO sheets with a single-layer thickness less than 1 nm are undoubtedly a preferred choice since there exist plenty of hydrophilic oxygen groups on the surface, for instance, hydroxyl and carboxyl groups. After GO decoration, the surface became superhydrophilic in air; whereas it was superoleophobic under water. The contact angle CA of a *n*-hexane droplet

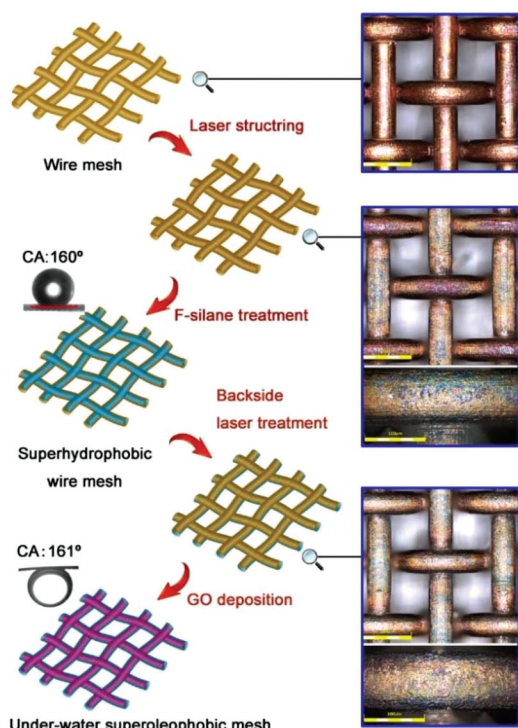


Fig. 1 Schematic illustration of the fabrication procedures of a Janus wire mesh. The insets are confocal laser scanning microscopy (CLSM) images of pristine Cu wire mesh, and the laser structured wire mesh observed from both sides, as well as water CA in air and oil (*n*-hexane) CA in water.

could reach 161° , indicating the very good anti-oil property under water. In this way, a Janus wire mesh that possesses different micronanostructures and surface chemical compositions on the two sides was fabricated. It contains a superhydrophobic/superoleophilic side and a superhydrophilic/under-water superoleophobic side.

Characterizations of the Janus mesh

We observed the surface micronanostructures on both sides of the Janus wire mesh by scanning electron microscopy (SEM). For a pristine Cu wire mesh, the surface is smooth (ESI, Fig. S1†). However, after femtosecond laser processing, the surface of the microwires became very rough. Fig. 2a–d show the SEM images of the laser structured and fluorosilane modified surface. A rough surface can be clearly identified from the images. Fig. 2c confirms the formation of LIPSS on the surface, and the period of the nanoripples is estimated to be ~ 900 nm. Previous results reported by us and other groups have proved the formation mechanism of LIPSS. Briefly, upon irradiation with multiple linearly polarized femtosecond laser pulses, low spatial frequency LIPSS with spatial periods comparable to the laser irradiation wavelength would form due to the optical interference of the incident laser radiation with a surface electromagnetic wave generated on the rough surface during the laser irradiation.^{26–31} Interestingly, after laser processing, the wire mesh exhibits a brilliant structural colour

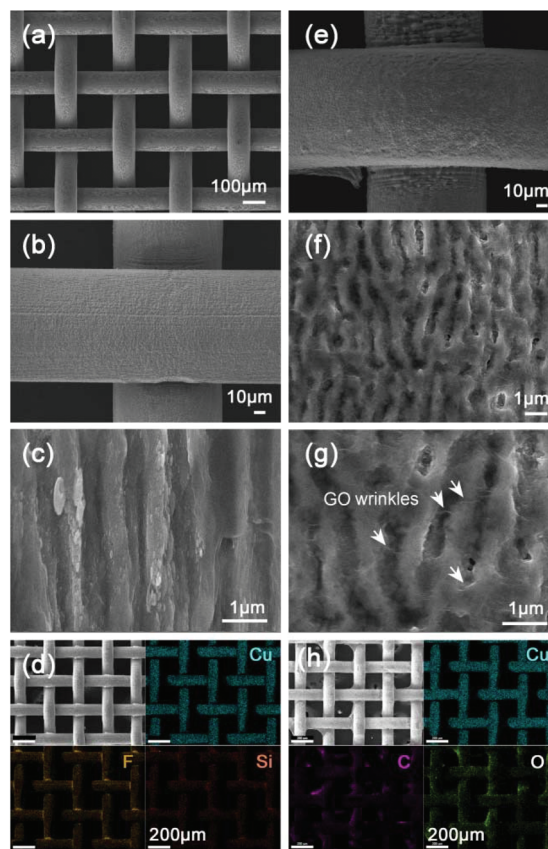


Fig. 2 SEM images of laser structured wire meshes. (a) Laser structured and fluorosilane modified wire mesh fabricated under a high laser intensity (580 mW, 7.39×10^6 mJ cm⁻²); (b) magnified SEM image; (c) SEM image of the surface LIPSS; (d) SEM image and elemental maps of the fluorosilane modified wire mesh; (e) SEM image of the laser structured and GO modified back side (treated under a relatively low laser intensity, 100 mW, 12.74×10^5 mJ cm⁻²); (f, g) magnified SEM image of the surface. GO could be identified from the wrinkles. (h) SEM image and elemental maps of the GO modified wire mesh.

due to the formation of LIPSS (ESI, Fig. S2†). To confirm the presence of fluorosilane on the mesh surface, elemental maps were collected. Elements of Cu, Si and F could be clearly observed, indicating that the surface of the wire mesh is homogeneously modified by fluorosilane.

Actually, the formation of LIPSS structures is dominated by both exposure conditions and material properties. Thus, we can easily tune the surface structures by altering the laser processing parameters, such as the fluence per pulse, the spatial intensity distribution, the cumulative exposure dose (number of pulses), the scanning step length and the polarization direction. In this work, to mimic the fish scale structures, we simply altered the laser intensity when treating the back side of the wire mesh. Fig. 2e and h show the SEM images of the back side (laser structured wire mesh decorated with GO). Unlike the LIPSS formed under a relatively high laser intensity (580 mW, 7.39×10^6 mJ cm⁻²), a worm-like LIPSS appeared after a low-intensity laser treatment (100 mW, 12.74×10^5 mJ cm⁻²). Even after coating with a thin layer of GO, the struc-

ture could be still well identified from the surface. The GO layer could be easily observed from the corners of the wires (Fig. 2e). Additionally, on the surface of the microwires, there exist some wrinkles between the gaps of the ripples, which also suggests the presence of GO. Elemental maps of carbon and oxygen further confirm that a continuous and homogeneous GO layer formed on the surface (Fig. 2h).

In addition to the surface morphologies, we also investigated the surface chemical compositions of the two sides by X-ray photoelectron spectroscopy (XPS). Fig. 3 shows the C 1s XPS spectra of the Janus mesh. On the surface of the fluorosilane modified side (Fig. 3a), carbon atoms that were bound to fluorine atoms (290.8 eV, $-\text{CF}_2$ and 292.7 eV, $-\text{CF}_3$) and silicon atoms (281.8 eV) could be clearly observed, respectively. The XPS results indicate that the fluorosilane is well modified on one side. The presence of fluorosilane on the surface can further lower the surface energy and increase the hydrophobicity. On the surface of the GO coating side (Fig. 3b), we observed typical C 1s XPS spectra of GO. The C 1s XPS spectra of GO can be deconvoluted into three peaks at 284.7 eV (C-C, nonoxygen ring), 286.7 eV (C-O, hydroxyl and epoxy carbon), and 288.2 eV (C=O, carbonyl), respectively. The content of oxygen atoms is $\sim 30.08\%$. The FT-IR spectra (Fig. S3†) further confirm the presence of oxygen containing groups (OCGs).

Characteristic vibration bands including a strong C=O peak (1740 cm^{-1}), an O-H deformation peak around 1420 cm^{-1} , a C-OH stretching peak around 1230 cm^{-1} and a C-O stretching peak around 1050 cm^{-1} could be clearly identified. The oxygen groups are quite helpful in achieving superhydrophilicity in air and the superoleophobicity under water.

Surface wettability of the Janus mesh

The surface wettability of the two sides of the Janus wire mesh were tested using static water/oil droplet contact angle (CA) and dynamic sliding angle (SA), respectively (Fig. 4). On the GO side, the surface is superhydrophilic in air due to the presence of abundant hydrophilic oxygen groups. When a water droplet gets in touch with the surface, it spreads out, rapidly (Fig. 4a). The superhydrophilicity in air also makes the surface superoleophobic under water. The SA of a CCl_4 droplet is measured to be $\sim 2^\circ$, indicating its superior underwater superoleophobicity (Fig. 4b). To further investigate the underwater superoleophobic property towards different organic oils, the underwater CAs of a series of organic reagents, including carbon tetrachloride, trichloromethane, bean oil, *n*-heptane, *n*-hexane, methylbenzene, acetic ether and *n*-butyl acetate, were measured (Fig. 4c). All of these oil droplets exhibit large CAs ($>155^\circ$), indicating the underwater superoleophobic

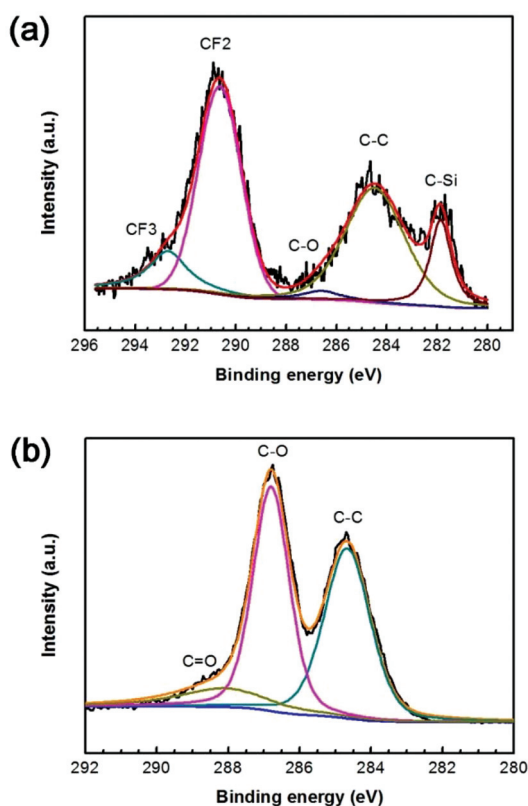


Fig. 3 C 1s XPS spectra of the Janus mesh. (a) C 1s XPS spectrum of the fluorosilane modified side; (b) C 1s XPS spectrum of the GO modified side.

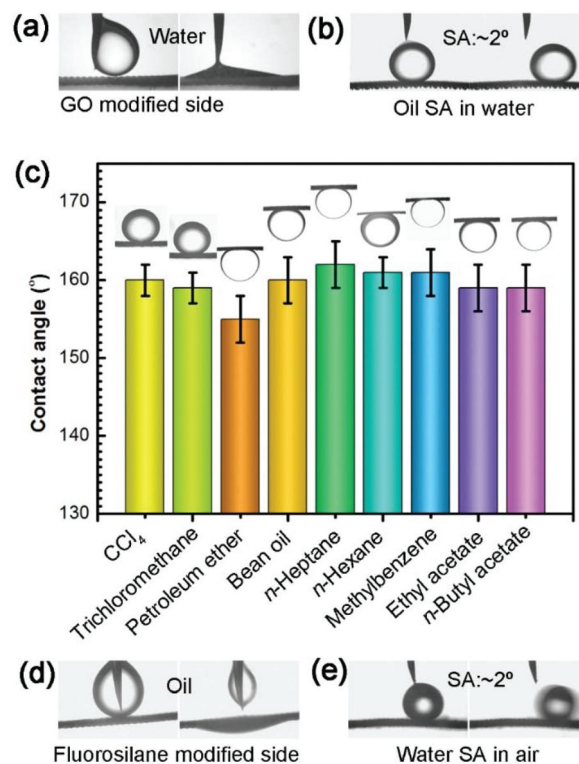


Fig. 4 (a) Water CA in air measured from the GO modified side; (b) under water SA of a CCl_4 droplet measured from the GO modified side; (c) CAs of various oil droplets measured from the GO modified side; (d) oil CA in air measured from the fluorosilane modified side; and (e) water droplet SA in air measured from the fluorosilane modified side.

properties. Besides, the mesh shows no selectivity towards different oils. It could be used for the separation of any oil species that are insoluble in water.

The fluorosilane modified side of the Janus mesh shows different wettabilities. As shown in Fig. 4d, the surface is superoleophilic in air. An oil droplet (CCl_4) would pass through the mesh easily, since both of the two sides are superoleophilic in air. However, it shows a Cassie state superhydrophobicity in air. A water droplet CA can reach $\sim 160^\circ$; and the SA is only $\sim 2^\circ$. Considering the distinct wettability on the two sides of the wire mesh, a Janus mesh is formed. The distinct wettability on the two sides make the Janus mesh workable in oil/water separation.

Oil/water separation and mechanisms

To evaluate the oil/water separation capability of the Janus mesh in two different cases, light oil on water and heavy oil beneath water, we sandwiched the Janus mesh between two plastic tubes and prepared a self-made oil/water separation setup. Fig. 5a shows the separation process of a bean oil and water mixture. We first placed the fluorosilane modified surface upwardly. In this case, a superhydrophobic surface comes into contact with the water/oil mixture first. In our experiments, we found that the intrusion pressure plays a very important role in the gravity-driven oil/water separation. The hydrostatic pressure should be large enough to induce the

separation. Herein, the intrusion pressure, ΔP , can be described as follows:³²

$$\Delta P = \frac{2\gamma}{R} = -l\gamma \frac{\cos \theta}{A}$$

where γ is the interfacial tension; l is the perimeter of the pore; R is the radius of the meniscus; A is the pore area, and θ_1 is the advancing CA. Fig. 5d shows the schematic illustration of this process. When water comes into contact with the superhydrophobic surface, the hydrostatic pressure pushes the water to permeate the mesh, while the hydrophobic force provides an opposite force, resisting the permeation. If the hydrostatic pressure is not large enough, the mixture cannot permeate the mesh at all due to its superhydrophobicity. Clearly, θ_1 is larger than 90° , so $\Delta P_1 > 0$ (Fig. 5d). If the hydrostatic pressure is large enough, ΔP_1 could be conquered. When water permeates deeply into the mesh pores and gets in touch with the hydrophilic region beneath, it would pass through the mesh due to the capillary effect. After water passes through the mesh, a water layer would form on the superhydrophilic surface beneath. When the oil comes in contact with the mesh, it would wet the superhydrophobic surface since $\theta' < 90^\circ$ and $\Delta P' < 0$. However, the oil cannot permeate the mesh, because when the interface reaches the superhydrophilic/underwater superoleophobic region, θ_2 becomes larger than 90° and $\Delta P_2 > 0$. In this regard, the mesh can support a certain pressure of the oil.

In the case of a heavy oil, the GO modified side should be put upwardly, and thus oil first contacts the mesh (Fig. 5b). Since both the GO coated mesh and the back side (fluorosilane modified mesh) are oleophilic in air, the oil could wet the surface and permeate easily, $\theta_3 < 90^\circ$, $\Delta P_3 < 0$ (Fig. 5e). When the oil passes through the mesh and water comes in contact with the GO coated mesh, water would wet the superhydrophilic surface since $\theta'' < 90^\circ$ and $\Delta P'' < 0$. However, water cannot permeate the mesh, because when the interface reaches the superhydrophobic region, θ_4 becomes larger than 90° , thus $\Delta P_4 > 0$. The mesh can support a certain pressure of water. By simply testing the separation of different oil/water mixtures, we found that the Janus mesh is workable for both of these cases: light oil and heavy oil. Selective permeation is achieved if a proper side of the Janus mesh is used. In addition to bean oil and water, CCl_4 and water mixtures, and some other oil/water mixtures including water and trichloromethane, methylbenzene and water, as well as *n*-heptane and water mixtures have been successfully separated (Fig. S4[†]). To prove the separation capacity, we measured the separation efficiency. As shown in Fig. 5f, the oil contents in water were found to be 0.02%, 0.01%, 0.02%, 0.03 and 0.05% by weight for the separation for bean oil/water, *n*-heptane/water, methylbenzene/water, water/perchloromethane and water/trichloromethane mixtures, respectively. Water residuals in bean oil, *n*-heptane, methylbenzene, perchloromethane and trichloromethane were found to be 0.04%, 0.02%, 0.05%, 0.07% and 0.08%, respectively. These results suggested that the Janus mesh shows very high separation efficiency for various oil/water mixtures. The Janus mesh

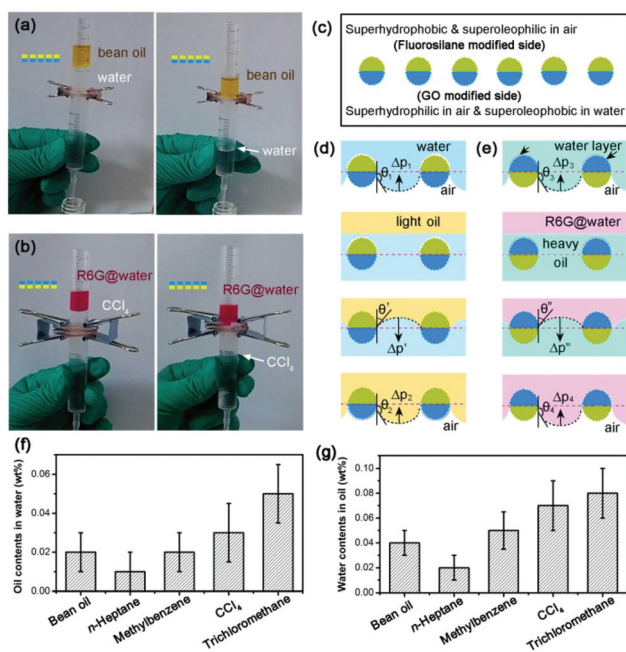


Fig. 5 Oil/water separation tests using the Janus meshes and the mechanism for the separation of different oil/water mixtures. (a) The separation of bean oil from water; (b) the separation of CCl_4 from R6G colored water; (c) scheme of the wettability of the Janus mesh; (d) mechanism for the separation process of light oil on water; (e) mechanism for the separation process of heavy oil underneath water; (f) separation efficiency of the Janus mesh, residual oil contents in water; and (g) contents of residual water in various oils.

is also very stable, and a continuous GO layer can be observed after the oil/water separation experiments (Fig. S5†).

Conclusions

In conclusion, a Janus mesh that is superoleophilic and superhydrophobic on one side, and superhydrophilic and underwater superoleophobic on the other side, has been successfully fabricated by laser structuring the surface followed by selective modification with fluorosilane and graphene oxide (GO), respectively. The wettability analysis confirmed that the combination of laser induced LIPSS and the post-modification with fluorosilane endows one side of the Janus mesh with superhydrophobicity; while the modification of the laser structured back side with GO makes the surface superoleophobic under water. The resultant Janus mesh is workable in the separation of different oil/water mixtures. We demonstrated the separation of several oil and water mixtures. The Janus mesh shows high separation efficiencies. Besides, the mechanism for oil/water separation has been discussed, in which the intrusion pressure was found critical for the separation process. The Janus mesh may hold great promise for efficient oil/water separation and contribute to the treatment of sewage.

Conflicts of interest

There are no conflicts to declare.

Acknowledgements

This work was supported by the National Key Research and Development Program of China and National Natural Science Foundation of China (NSFC) under Grants #2017YFB1104300, #61522503, #61376123, #61590930, and 51335008.

Notes and references

- J. Yong, F. Chen, Q. Yang, J. Huo and X. Hou, *Chem. Soc. Rev.*, 2017, **46**, 4168–4217.
- F. Chen, D. Zhang, Q. Yang, J. Yong, G. Du, J. Si, F. Yun and X. Hou, *ACS Appl. Mater. Interfaces*, 2013, **5**, 6777.
- Y. H. Zhao, M. Zhang and Z. K. Wang, *Adv. Mater. Interfaces*, 2016, **3**, 7.
- K.-C. Liu, Z.-Y. Zhang, C.-X. Shan, Z.-Q. Feng, J.-S. Li, C.-L. Song, Y.-N. Bao, X.-H. Qi and B. Dong, *Light Sci. Appl.*, 2016, **5**, e16136.
- W. Zhang, H. Zappe and A. Seifert, *Light Sci. Appl.*, 2014, **3**, e145.
- J. L. Yong, Y. Fang, F. Chen, J. L. Huo, Q. Yang, H. Bian, G. Q. Du and X. Hou, *Appl. Surf. Sci.*, 2016, **389**, 1148–1155.
- C. L. Hao, Y. H. Liu, X. M. Chen, J. Li, M. Zhang, Y. H. Zhao and Z. K. Wang, *Small*, 2016, **12**, 1825–1839.
- C. L. Yu, C. M. Yu, L. Y. Cui, Z. Y. Song, X. Y. Zhao, Y. Ma and L. Jiang, *Adv. Mater. Interfaces*, 2017, **4**, 5.
- H. G. Zhu, D. Y. Chen, W. An, N. J. Li, Q. F. Xu, H. Li, J. H. He and J. M. Lu, *Small*, 2015, **11**, 5222–5229.
- J. L. Yong, F. Chen, Q. Yang, H. Bian, G. Q. Du, C. Shan, J. L. Huo, Y. Fang and X. Hou, *Adv. Mater. Interfaces*, 2016, **3**, 7.
- R. Li, C. B. Chen, J. Li, L. M. Xu, G. Y. Xiao and D. Y. Yan, *J. Mater. Chem. A*, 2014, **2**, 3057–3064.
- G. Q. Li, H. Fan, F. F. Ren, C. Zhou, Z. Zhang, B. Xu, S. Z. Wu, Y. L. Hu, W. L. Zhu, J. W. Li, Y. S. Zeng, X. H. Li, J. R. Chua and D. Wu, *J. Mater. Chem. A*, 2016, **4**, 18832–18840.
- Z. W. Yu, F. F. Yun, Z. Y. Gong, Q. Yao, S. X. Dou, K. S. Liu, L. Jiang and X. L. Wang, *J. Mater. Chem. A*, 2017, **5**, 10821–10826.
- G. Q. Li, Y. Lu, P. C. Wu, Z. Zhang, J. W. Li, W. L. Zhu, Y. L. Hu, D. Wu and J. R. Chu, *J. Mater. Chem. A*, 2015, **3**, 18675–18683.
- G. Q. Li, Z. Zhang, P. C. Wu, S. Z. Wu, Y. L. Hu, W. L. Zhu, J. W. Li, D. Wu, X. H. Li and J. R. Chu, *RSC Adv.*, 2016, **6**, 37463–37471.
- J. Ni, C. Wang, C. Zhang, Y. Hu, L. Yang, Z. Lao, B. Xu, J. Li, D. Wu and J. Chu, *Light Sci. Appl.*, 2017, **6**, e17011.
- L. Feng, Z. Y. Zhang, Z. H. Mai, Y. M. Ma, B. Q. Liu, L. Jiang and D. B. Zhu, *Angew. Chem., Int. Ed.*, 2004, **43**, 2012–2014.
- B. Wang, W. X. Liang, Z. G. Guo and W. M. Liu, *Chem. Soc. Rev.*, 2015, **44**, 336–361.
- Q. L. Ma, H. F. Cheng, A. G. Fane, R. Wang and H. Zhang, *Small*, 2016, **12**, 2186–2202.
- Y. B. Peng and Z. G. Guo, *J. Mater. Chem. A*, 2016, **4**, 15749–15770.
- Y. F. Si and Z. G. Guo, *Chem. Lett.*, 2015, **44**, 874–883.
- P. S. Brown and B. Bhushan, *Philos. Trans. R. Soc., A*, 2016, **374**, 40.
- Y. Q. Liu, Y. L. Zhang, X. Y. Fu and H. B. Sun, *ACS Appl. Mater. Interfaces*, 2015, **7**, 20930–20936.
- Z. Cheng, B. Wang, H. Lai, P. Liu, D. Zhang, D. Tian, H. Liu, X. Yu, B. Sun and K. Sun, *Chem. – Asian J.*, 2017, **12**, 2085–2091.
- H. C. Yang, J. Hou, V. Chen and Z. K. Xu, *Angew. Chem., Int. Ed.*, 2016, **55**, 13398–13407.
- M. Malinauskas, A. Zukauskas, S. Hasegawa, Y. Hayasaki, V. Mizeikis, R. Buividas and S. Juodkasis, *Light: Sci. Appl.*, 2016, **5**, 14.
- S. Juodkasis, *Nat. Photonics*, 2016, **10**, 499–501.
- Y. Y. Huo, T. Q. Jia, D. H. Feng, S. Zhang, J. K. Liu, J. Pan, K. Zhou and Z. R. Sun, *Laser Phys.*, 2013, **23**, 7.
- J. Bonse, A. Rosenfeld and J. Kruger, *J. Appl. Phys.*, 2009, **106**, 5.
- G. D. Tsibidis, E. Stratakis, P. A. Loukakos and C. Fotakis, *Appl. Phys. A: Mater. Sci. Process.*, 2014, **114**, 57–68.
- G. Lozano, S. R. K. Rodriguez, M. A. Verschuuren and J. Gomez Rivas, *Light Sci. Appl.*, 2016, **5**, e16080.
- J. P. Youngblood and T. J. McCarthy, *Macromolecules*, 1999, **32**, 6800–6806.